

Total electron-scattering cross sections of pyrimidine

W. Y. Baek,¹ A. Arndt,¹ M. U. Bug,^{1,2} H. Rabus,¹ and M. Wang¹

¹*Physikalisch-Technische Bundesanstalt, Bundesallee 100, 38116 Braunschweig, Germany*

²*Center for Medical Radiation Physics, University of Wollongong, Wollongong, NSW 2522, Australia*

(Received 18 June 2013; published 9 September 2013)

Total electron-scattering cross sections of pyrimidine, the basic component for the nucleic bases cytosine and thymine, were measured for electron energies from 5 eV to 1 keV using the linear transmission method. The measured results were compared to semiempirical data obtained by means of the additivity rule and to experimental data for benzene since it has a similar ring structure and the same number of valence electrons as pyrimidine. Furthermore, integral elastic and inelastic electron-scattering cross sections of pyrimidine were calculated by applying the spherical complex optical potential model. The sum of both cross sections agrees reasonably well with the experimental total electron-scattering cross sections of pyrimidine in the energy range from 20 eV to 1 keV. The experimental data are, however, significantly lower than the theoretical cross sections when including the contribution of rotational excitations to the electron scattering.

DOI: [10.1103/PhysRevA.88.032702](https://doi.org/10.1103/PhysRevA.88.032702)

PACS number(s): 34.80.Bm

I. INTRODUCTION

It is a general consensus that DNA is the primary target for cellular damage induced by ionizing radiation [1]. When penetrating tissues, ionizing radiation causes cellular damage either by a direct excitation and ionization of the DNA or via secondary electrons that further undergo interactions with the DNA in the lateral environment of the primary radiation track. The secondary electrons are responsible for a significant part of the radiation damage. Their contribution to the radiation damage is predominant in the case of low linear energy transfer (LET) radiations.

Since an experimental investigation of the initial physical action of ionizing radiation at cellular levels is not yet feasible, Monte Carlo simulations are commonly applied to specify the initial radiation damage. For such simulations, the total electron-scattering cross sections (TCS) of DNA constituents play an important role. As the sum of all interaction cross sections, they represent the upper limit for partial scattering cross sections and can therefore be employed to check the consistency of compiled data sets. Total electron-scattering cross sections are also often used to put relative electron-scattering cross sections on an absolute scale [2], and in Monte Carlo simulations they are required to determine the mean distance between two subsequent interaction points.

Few experiments have been carried out to determine the TCS of molecules which serve as the models of building blocks of DNA. Up to now, the most attention has been paid to tetrahydrofuran (THF), which is used as the model molecule for the deoxyribose in the backbone of the DNA. Baek *et al.* [2] determined the TCS of THF for electron energies between 6 eV and 1 keV using the same experimental setup as in the present work. Zecca *et al.* [3] measured the TCS of THF for low electron energies. Mozejko *et al.* [4] reported the experimental TCS of THF for electron energies from 1 to 370 eV and Fuss *et al.* [5] measured those in the intermediate and high energy regions.

Regarding the TCS of nucleic bases for electron scattering, no experimental data have been published yet. Recently, Zecca *et al.* [6] measured the TCS of pyrimidine, the basic component for the nucleic bases cytosine and thymine, for positrons in the

energy range from 0.3 to 45 eV. They calculated the TCS of pyrimidine for electrons in the energy range between 1 eV and 10 keV using the independent-atom screened additivity rule [7,8].

In the present work, the TCS of pyrimidine were measured for electron energies from 5 eV to 1 keV using a linear transmission experiment. The experimental data are compared to theoretical TCS which were calculated by applying the spherical complex optical potential (SCOP) model [9]. Using this model, the integral elastic and inelastic electron-scattering cross sections of pyrimidine were computed for electron energies between 10 eV and 1 keV. Furthermore, the total ionization cross sections of pyrimidine were determined by means of the binary encounter Bethe (BEB) model [10].

II. EXPERIMENT

The measurements were carried out using the linear transmission device described previously [11]. It consists of an electron gun, a scattering chamber, and an electron energy analyzer. The electron gun, equipped with a hairpin tungsten filament, delivered stable electron beams in the energy range from 20 eV to 5 keV. An electrostatic lens and two orthogonal pairs of deflection plates were used to focus and align the electron beam, respectively. The scattering chamber consisted of a hollow metallic cylinder mounted in a vacuum recipient. The symmetry axis of the scattering chamber was set perpendicular to that of the electron beam. Two circular apertures on the cylinder shell defined the electron beam direction. The diameter of both apertures and of the scattering chamber amounted to 0.5 and 132 mm, respectively. The apertures were electrically isolated from the scattering chamber for the monitoring of the change of the incident electron beam current.

To enable the measurement of TCS below 20 eV, the scattering chamber was electrically isolated so that a negative dc bias voltage U_{ch} could be applied [11]. This leads to the reduction of the incident electron energy T_0 by the amount of eU_{ch} at the entrance aperture. In this case, the electrons undergo collision processes in the scattering chamber at the reduced energy $T = T_0 - e|U_{\text{ch}}|$ and those transmitted

without interaction regain their initial energy on the path between the exit aperture and the electron energy analyzer.

The electron beam underwent collision processes with gaseous pyrimidine in the scattering chamber, leading to an attenuation of the electron current along the beam direction. The electron beam leaving the scattering chamber entered an electron energy analyzer which discriminated unscattered electrons from electrons scattered inelastically in the forward direction. The electron energy analyzer was of hemispherical condenser design with a mean radius of 100 mm and a deflection angle of 150° . A channel electron multiplier, mounted at the end of the analyzer, was used for the detection of electrons.

The geometrical solid angle subtended by the detector varied from 7×10^{-4} sr at high electron energies to 1.1×10^{-3} sr below 20 eV. The energy resolution (FWHM) was adjusted by changing the retardation voltage applied to the entrance slit of the analyzer [12]. The relative energy resolution was better than 0.25%. The absolute value of the energy resolution was smaller than 0.5 eV at electron energies below 100 eV and amounted to about 1 eV at 1 keV. The whole electron beam path was passively shielded against the residual earth magnetic field as well as other electromagnetic disturbances by means of a permalloy housing. The major part of the external magnetic field was actively compensated by three orthogonal pairs of Helmholtz coils surrounding the scattering chamber.

The scattering chamber was connected to a gas source via a regulating valve with an adjustable leak rate from 10^{-9} mbar l/s to 10^{-1} mbar l/s. Before the introduction of the gas, the scattering chamber was evacuated down to a residual pressure lower than 10^{-6} mbar. The vapor of liquid pyrimidine with a stated purity of 99.9% was used as gas source. At room temperatures of higher than 28°C , the vapor pressure of pyrimidine was sufficiently high for the experiment.

The gas pressure in the scattering chamber was measured by means of a capacitance manometer which had been calibrated at the vacuum metrology section of Physikalisch-Technische Bundesanstalt in Berlin, Germany, in order to correct for the thermal transpiration effect [13]. The calibration was carried out for several light gases such as N_2 and CH_4 in the pressure range between 10^{-3} and 1 mbar. The greatest deviation between the reading of the capacitance manometer used in this work and the primary standard was found in the pressure region around 10^{-3} mbar. In the pressure region around 1 mbar, there was almost no difference between both values. Since the typical gas pressure in the present experiment lay between 10^{-3} and 10^{-2} mbar, a disregard of the thermal transpiration effect would lead to a lowering of the experimental results by about 3%.

As the correction factor Γ , defined as the ratio of the reading value p_R of the capacitance manometer to the pressure standard p_N , was not known for pyrimidine, it was estimated using the empirical equation for the thermal transpiration effect proposed by Takaishi and Sensui [14]:

$$\begin{aligned} & [1 - (p/p_m)]/[1 - (T_1/T_2)^{1/2}] \\ & = 1/(AX^2 + BX + CX^{1/2} + 1). \end{aligned} \quad (1)$$

T_1 and p are the temperature and pressure in the chamber, respectively, and p_m is the pressure in the manometer gauge

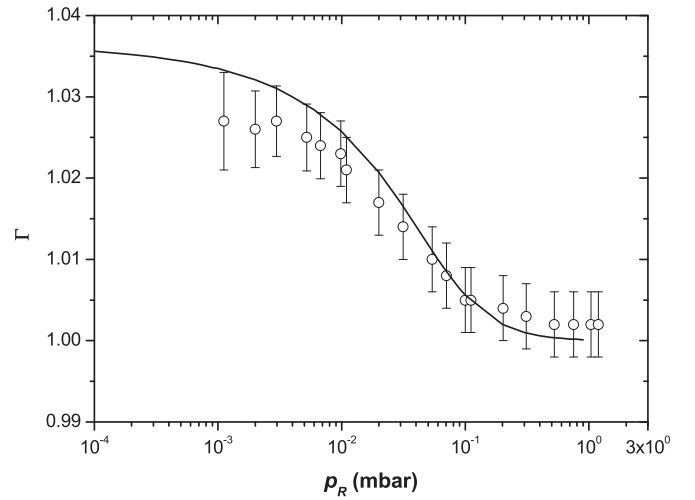


FIG. 1. Pressure correction factor Γ for pyrimidine as a function of the reading p_R of the capacitance manometer. For comparison, the experimental corrections factors (\circ) of methane are shown.

held at T_2 with $T_2 > T_1$. Here, the ratio p_m/p corresponds to the correction factor Γ . The quantity X is equal to the product of p_m and the diameter d of the connection line between the scattering chamber and the manometer gauge along which a temperature gradient occurs: $X = p_m d$. The constants A , B , and C are related to gas kinetic collision cross sections. The correction factor for pyrimidine was estimated using the gas kinetic collision cross sections of benzene (C_6H_6) whose molecular diameter and structure is similar to that of pyrimidine. Here, the gas kinetic collision cross section of benzene was determined from its dynamic viscosity value [15]. Figure 1 shows the estimated correction factor for pyrimidine in comparison to that of methane.

The determination of TCS σ_t was based on Beer's attenuation law taking into account the secondary effects:

$$c = c_0 \left[\exp(-\sigma_t n_F) - \int n(z) dz \int_{\Delta\Omega(z)} \frac{d\sigma}{d\Omega} d\Omega \right], \quad (2)$$

where c_0 and c are the electron count rate of the channel electron multiplier without and with the gas in the scattering chamber, respectively. The quantity n_F is the number of molecules per area crossed by the electron beam and is given, when considering the inhomogeneity of the number density due to the gas streaming out through the apertures, by the integral of the number density distribution $n(z)$ over the electron beam trajectory:

$$n_F = \int n(z) dz \equiv k_1 n_0 L_0. \quad (3)$$

In Eq. (3), n_0 is the number density in the static case where there is no gas flow through the apertures and L_0 is the diameter of the scattering chamber. In the static case, n_0 can be determined from the ideal gas law $n_0 = p/(k_B T_1)$, where the gas temperature T_1 is assumed to be equal to the room temperature measured with a uncertainty smaller than 1 K.

The second integral on the right-hand side of Eq. (2) corrects for the signal contribution from electrons that underwent scattering processes but were counted due to the finite

detection solid angle $\Delta\Omega(z)$. This contribution is proportional to the differential electron-scattering cross section $d\sigma/d\Omega$ depending on the scattering angle and on the electron energy. In the present work, $d\sigma/d\Omega$ was set to be equal to the differential elastic-scattering cross section $d\sigma_{el}/d\Omega$; in other words, the rotational and vibrational excitations whose transition energies are smaller than the energy resolution of the electron energy analyzer were not taken into account in $d\sigma/d\Omega$. The consequence of disregarding these excitation processes is discussed below in the comparison of the experimental data with theoretical values. The z -dependent detector solid angle $\Delta\Omega(z)$ can be approximated by an average value, as the distance between the center of the scattering chamber and the detector, which was 384 mm, was much greater than the diameter of the scattering chamber:

$$\int n(z)dz \int_{\Delta\Omega(z)} \frac{d\sigma}{d\Omega} d\Omega \approx \frac{d\sigma_{el}}{d\Omega} \Delta\bar{\Omega} \int n(z)dz = \frac{d\sigma_{el}}{d\Omega} \Delta\bar{\Omega} k_1 n_0 L_0 \equiv \Delta\bar{\sigma}_{el} k_1 n_0 L_0. \quad (4)$$

In Eq. (4), $\Delta\bar{\Omega}$ is the detector solid angle subtended at the position $z = L_0/2$. In the present experimental arrangement, $\Delta\bar{\sigma}_{el}$ is in the order of 1% of σ_t . Therefore, Eq. (2) can be approximately rewritten as

$$\ln\left(\frac{c}{c_0}\right) \approx k_1 n_0 L_0 (\sigma_t - \Delta\bar{\sigma}_{el}). \quad (5)$$

According to Eq. (5), the TCS σ_t can be determined by recording the count rate c as a function of the gas number density n_0 or the chamber pressure p , if the values of k_1 and $\Delta\bar{\sigma}_{el}$ are known. The correction factor k_1 , which accounts for the pressure drop in the vicinity of the apertures and for the additional beam attenuation in the effusing gas stream, was estimated using the calculations of Nelson and Colgate [16]. The resulting value of k_1 for the apertures and the scattering chamber used in this work amounted to 0.99.

The value of $\Delta\bar{\sigma}_{el}$ was estimated by means of the differential elastic electron-scattering cross sections $d\sigma_{el}/d\Omega$ calculated using the modified independent-atom model [17]. In the present work, the pressure in the scattering chamber varied between the residual pressure of about 1.0×10^{-6} mbar and a maximal pressure depending on the electron energy. The maximal pressure value was adjusted such that the beam attenuation ratio c/c_0 did not fall below 0.6 to keep the signal contribution arising due to multiple scattering effects below 1%.

A considerable increase of the electron beam current was observed when pyrimidine vapor was introduced into the scattering chamber. This increase arises due to the chemical reaction of the tungsten filament with the pyrimidine gas streaming out through the entrance aperture of the scattering chamber. In order to take into account the change of the electron emission due to the gas exposure of the filament, the primary electron beam current I_p was measured on the entrance aperture of the scattering chamber. The TCS $\sigma_t(T)$ was then obtained by a linear fit of $\ln[(c/I_p)/(c_0/I_{p,0})]$ versus $n_0 L_0$, where $I_{p,0}$ is the primary beam current if no gas is present in the scattering chamber. The slope σ_0 of the linear fit is given by Eq. (5) and equal to $k_1(\sigma_t - \Delta\bar{\sigma}_{el})$. The

measurement was repeated ten times for each electron energy to reduce the uncertainties arising from statistical fluctuations. The TCS σ_t of pyrimidine was then determined using the mean value $\bar{\sigma}_0$ of the ten measurements:

$$\sigma_t = \bar{\sigma}_0/k_1 + \Delta\bar{\sigma}_{el}. \quad (6)$$

The standard uncertainty $u(\sigma_t)$ of the experimental TCS was calculated according to the Guide to the Expression of Uncertainty in Measurements [18]:

$$u^2(\sigma_t) = \left(\frac{\partial\sigma_t}{\partial k_1} \delta k_1\right)^2 + \left(\frac{\partial\sigma_t}{\partial \bar{\sigma}_0} \delta \bar{\sigma}_0\right)^2 + \left(\frac{\partial\sigma_t}{\partial (\Delta\bar{\sigma}_{el})} \delta(\Delta\bar{\sigma}_{el})\right)^2 + \left(\frac{\partial\sigma_t}{\partial T} \delta T\right)^2, \quad (7)$$

where only the main uncertainty sources are taken into account. The uncertainty δk_1 amounted to 1×10^{-2} and the relative value of the uncertainty $\delta \bar{\sigma}_0$ varied between 1% and 10% depending on the electron energy. The uncertainty of $\Delta\bar{\sigma}_{el}$ is mainly given by that of $d\sigma_{el}/d\Omega$ of pyrimidine. The relative uncertainty $\delta(\Delta\bar{\sigma}_{el})/\Delta\bar{\sigma}_{el}$, estimated by comparing the calculated $d\sigma_{el}/d\Omega$ with available experimental data [19,20], amounted to 50%. The derivative $\partial\sigma_t/\partial T$ was determined using the cubic interpolation of the experimental results and δT was set equal to the uncertainty of the calibration of the electron energy that has been carried out before by means of the retarding field method [11,21].

III. THEORETICAL METHODS

In addition to the measurement, the TCS of pyrimidine were calculated by means of the SCOP model [9]. This model is based on the fixed-nuclei approximation and describes the electron scattering by means of a complex potential $V_{opt}(\vec{r})$ given by

$$V_{opt}(\vec{r}) = V_R(\vec{r}) + iV_{abs}(\vec{r}), \quad (8)$$

where the real and imaginary parts of the potential account for elastic and inelastic scattering, respectively. The real part $V_R(\vec{r})$ consists of the static potential $V_{st}(\vec{r})$, the exchange potential $V_{ex}(\vec{r})$, and the correlation-polarization potential $V_{pol}(\vec{r})$:

$$V_R(\vec{r}) = V_{st}(\vec{r}) + V_{ex}(\vec{r}) + V_{pol}(\vec{r}). \quad (9)$$

The imaginary part $V_{abs}(\vec{r})$ describes the dissipation of incoming electron waves into the inelastic channels such as ionization and excitation.

In the SCOP model, $V_{opt}(\vec{r})$ is at first expanded around the center of mass of the molecule using symmetry-adapted functions [22]:

$$V_{opt}^{p\mu}(\vec{r}) = \sum_{l,h} v_{lh}(r) X_{lh}^{p\mu}(\hat{r}), \quad (10)$$

where $p\mu$ designates the particular irreducible representation of the molecular point group in the ground state, h denotes a specific basis at an angular momentum l for $p\mu$, r is the distance from the center of mass of the molecule, \hat{r} is the unit vector of \vec{r} , and v_{lh} is the corresponding expansion coefficient. For closed-shell nonlinear molecules such as pyrimidine, the ground-state symmetry $p\mu$ is equal to the irreducible

representation 1A_1 and the symmetry-adapted function $X_{lh}^{A_1}(\hat{r})$ can be represented as a linear combination of real spherical harmonics $S_{lm}(\hat{r})$ [23]:

$$X_{lh}^{A_1}(\hat{r}) = \sum_{m=0}^l b_{lhm}^{A_1} S_{lm}(\hat{r}). \quad (11)$$

The values of the coefficients $b_{lhm}^{A_1}$ are given by the character table of the corresponding irreducible representation.

The main feature of the SCOP model [9] is that only the isotropic term in the multipole expansion, i.e., the first term with $l = 0$ and $h = 0$, is considered. In this case, the optical potential $V_{\text{opt}}^{\text{SCOP}}(\vec{r})$ can be written as

$$V_{\text{opt}}^{\text{SCOP}}(\vec{r}) = v_{01}(r)b_{010}^{A_1}S_{00}(\hat{r}) = v_{01}(r)/\sqrt{4\pi}. \quad (12)$$

As the following equation shows, the consideration of only the isotropic term is equivalent to averaging $V_{\text{opt}}(\vec{r})$ over the entire solid angle:

$$\begin{aligned} \bar{V}_{\text{opt}}(r) &= \frac{\int V_{\text{opt}}(\vec{r})d\Omega}{4\pi} = \frac{\sqrt{4\pi} \int V_{\text{opt}}(\vec{r})S_{00}(\hat{r})d\Omega}{4\pi} \\ &= \frac{\int \sum_{l,h} v_{lh}(r) \sum_{m=0}^l b_{lhm}^{p\mu} S_{lm}(\hat{r})S_{00}(\hat{r})d\Omega}{\sqrt{4\pi}} \\ &= \frac{v_{01}(r)}{\sqrt{4\pi}} = V_{\text{opt}}^{\text{SCOP}}(\vec{r}), \end{aligned} \quad (13)$$

where use was made of the orthogonality relation of the spherical harmonics $\int S_{lm}(\hat{r})S_{l'm'}(\hat{r})d\Omega = \delta_{ll'}\delta_{mm'}$. The above averaging can be interpreted as the averaging of the interaction potential over all molecular orientations which are randomly distributed in the gas beam.

All four potentials given on the right-hand side of Eqs. (8) and (9) depend on the electron density distribution $\rho(\vec{r})$, which was calculated by means of the quantum chemical program GAUSSIAN 09 [24] deploying the 6-311G** basis sets. The static and correlation-polarization potentials $V_{\text{st}}(\vec{r})$ and $V_{\text{pol}}(\vec{r})$, respectively, were then computed from this electron density distribution with the help of the library SCELIB [23]. It should be noted that the calculation of $V_{\text{pol}}(\vec{r})$ was based on the formulations for the VCP polarization potential given in Ref. [23]. The exchange potential $V_{\text{ex}}(\vec{r})$ was obtained by the application of the following formula which was derived from the free electron gas model of Hara [25]:

$$V_{\text{ex}}(\vec{r}) = -\frac{2}{\pi}k_F(\vec{r}) \left(\frac{1}{2} + \frac{1-\zeta^2}{4\zeta} \ln \left| \frac{1+\zeta}{1-\zeta} \right| \right) \quad (14)$$

with $k_F(\vec{r}) = [3\pi^2\rho(\vec{r})]^{1/3}$ and $\zeta(\vec{r}) = (k^2 + 2I + k_F^2)^{1/2}/k_F$, where k is the initial momentum of the incident electron and I is the ionization potential in atomic units.

The absorption potential that is dependent on the electron energy T was determined using the quasifree-scattering model described in detail by Staszeweska *et al.* [26,27]. In this model, $V_{\text{abs}}(\vec{r})$ is given by

$$\begin{aligned} V_{\text{abs}}(\vec{r}) &= -\rho(\vec{r})\sqrt{2(T - V^{\text{se}})} \left(\frac{4\pi}{10k_F^3 T} \right) H \\ &\times (k^2 - k_F^2 - 2\Delta)(A_1 + A_2 + A_3), \end{aligned} \quad (15)$$

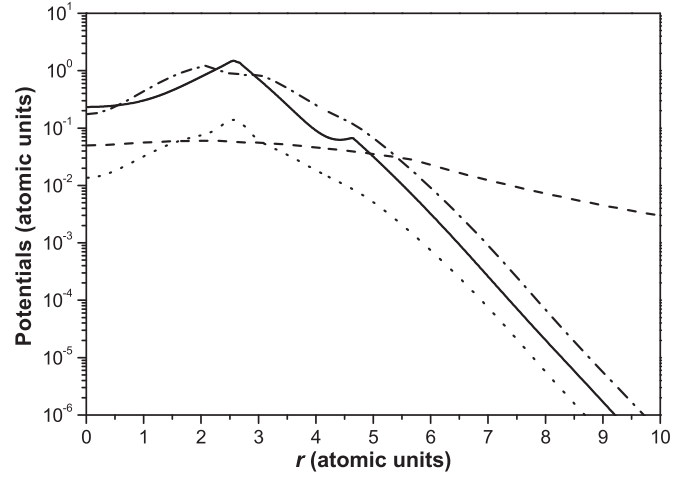


FIG. 2. Spherically averaged potentials for 100-eV electrons used for the calculation of electron-scattering cross sections by means of the SCOP model [9]: (—) \bar{V}_{st} , (····) \bar{V}_{ex} , (---) \bar{V}_{pol} , and (— · — ·) \bar{V}_{abs} .

where $V^{\text{se}}(\vec{r}) = V_{\text{st}}(\vec{r}) + V_{\text{ex}}(\vec{r})$, $H(x)$ is the Heaviside step function, such that $H(x) = 1$ for $x \geq 0$ and $H(x) = 0$ for $x < 0$, and Δ is the mean excitation energy. The terms A_1 , A_2 , and A_3 are defined as

$$\begin{aligned} A_1 &= \frac{5k_F^3}{2\Delta}, \quad A_2 = \frac{k_F^3[5(k^2 - k_F^2) + 2k_F^2]}{(k^2 - k_F^2)}, \\ A_3 &= H(2k_F^2 + 2\Delta - k^2) \frac{2(2k_F^2 + 2\Delta - k^2)^{5/2}}{(k^2 - k_F^2)}. \end{aligned} \quad (16)$$

Jain and Baluja [9] calculated the mean excitation energy Δ for a variety of molecules and found that the value of Δ is very close to the ionization potential in the most cases. Therefore, Δ was set equal to the ionization potential I of pyrimidine. Figure 2 depicts the spherically averaged potentials $\bar{V}_{\text{st}}(r)$, $\bar{V}_{\text{ex}}(r)$, $\bar{V}_{\text{pol}}(r)$, and $\bar{V}_{\text{abs}}(r)$ as functions of the distance from the center of mass of the molecule.

As $\bar{V}_{\text{opt}}(r)$ is spherically symmetric, the wave function of the scattered electrons can be determined by solving radial Schrödinger equations in combination with the partial wave expansion method:

$$\left[\frac{d^2}{dr^2} + k^2 - \frac{l(l+1)}{r^2} - 2\bar{V}_{\text{opt}}(r) \right] \varphi_l(r) = 0, \quad (17)$$

where k is the momentum of the incident electron and φ_l is the partial wave for the angular momentum quantum number l .

Equation (17) was solved by applying the variable phase approach [28], which transforms the complex second-order differential equation into two coupled nonlinear first-order differential equations. In this approach, the real part $\varepsilon_l(kr)$ and the imaginary part $\eta_l(kr)$ of the phase shift can be obtained from the following system of coupled differential equations:

$$\begin{aligned} \varepsilon_l' &= -\frac{1}{k} [\bar{V}_R(X^2 - Y^2) - 2\bar{V}_{\text{abs}}XY], \\ \eta_l' &= -\frac{1}{k} [\bar{V}_{\text{abs}}(X^2 - Y^2) + 2\bar{V}_RXY] \end{aligned} \quad (18)$$

with

$$\begin{aligned} X &= \cosh \eta_l (\hat{\eta}_l \sin \varepsilon_l - \hat{j}_l \cos \varepsilon_l), \\ Y &= \sinh \eta_l (\hat{\eta}_l \cos \varepsilon_l + \hat{j}_l \sin \varepsilon_l), \end{aligned} \quad (19)$$

where the phase shift fulfills the boundary conditions $\varepsilon_l(0) = 0$ and $\eta_l(0) = 0$. The functions $\hat{j}_l(kr)$ and $\hat{\eta}_l(kr)$ are the Riccati-Bessel functions. It should be noted that Eqs. (18) and (19) deviate from those found in literature [9,22,29–32] which, in contrast to our Eqs. (18) and (19), are inconsistent with the original formulas given in Ref. [28].

The phase shifts $\varepsilon_l(kr)$ and $\eta_l(kr)$ for $r \rightarrow \infty$ are related to the S matrix S_l via

$$S_l(k) = \exp[-2\eta_l] \exp[2i\varepsilon_l]. \quad (20)$$

The integral elastic σ_{el} , absorption σ_{abs} , and total σ_t cross sections can be calculated from the S matrix $S_l(k)$ by means of the following equations:

$$\begin{aligned} \sigma_{\text{el}}(k) &= \frac{\pi}{k^2} \sum_{l=0}^{l_{\text{max}}} (2l+1) |1 - S_l(k)|^2, \\ \sigma_{\text{abs}}(k) &= \frac{\pi}{k^2} \sum_{l=0}^{l_{\text{max}}} (2l+1) [1 - |S_l(k)|^2], \\ \sigma_t(k) &= \frac{2\pi}{k^2} \sum_{l=0}^{l_{\text{max}}} (2l+1) [1 - \text{Re} S_l(k)]. \end{aligned} \quad (21)$$

The values of $S_l(k)$ were obtained from the asymptotic values of $\varepsilon_l(kr)$ and $\eta_l(kr)$ via Eq. (20), where $\varepsilon_l(k)$ and $\eta_l(k)$ were determined by the numerical integration of Eq. (18) over r using the fourth-order Runge-Kutta method [33]. The integration was carried out until the relative change of the absolute value of the phase shift was smaller than 1.0×10^{-5} .

As mentioned above, the SCOP model [9] takes into account only the isotropic $l = 0$ term in the multipole expansion of $\bar{V}_{\text{opt}}(r)$. The disregard of the anisotropic terms with $l \geq 1$, however, can lead to a considerable underestimate of electron-scattering cross sections in the case of molecules with high dipole moments like pyrimidine since such molecules can be rotationally excited during the interaction with incident electrons.

Following the approach used by Jain [34], the contribution of rotational excitations to the electron-scattering cross section was calculated using the formula of Collins and Norcross [35] and incoherently added to the integral cross sections obtained using Eq. (21). According to the formula of Collins and Norcross [35], which is based on the first Born approximation for a rotating dipole, the integral cross section for rotational excitation is given by

$$\sigma_{\text{rot}}(j \rightarrow j') = \frac{8\pi}{3k^2} D_m^2 \frac{j'}{2j+1} \ln \frac{k+k'}{|k-k'|} \quad (22)$$

with

$$2k'^2 = 2k^2 - (E_{j'\tau} - E_{j\tau}), \quad (23)$$

where D_m is the molecular dipole moment and $E_{j\tau}$ is the energy of the rotational state ($j\tau$). The energy levels of the rotational states of pyrimidine, which is an asymmetric top molecule, were calculated by means of the computational

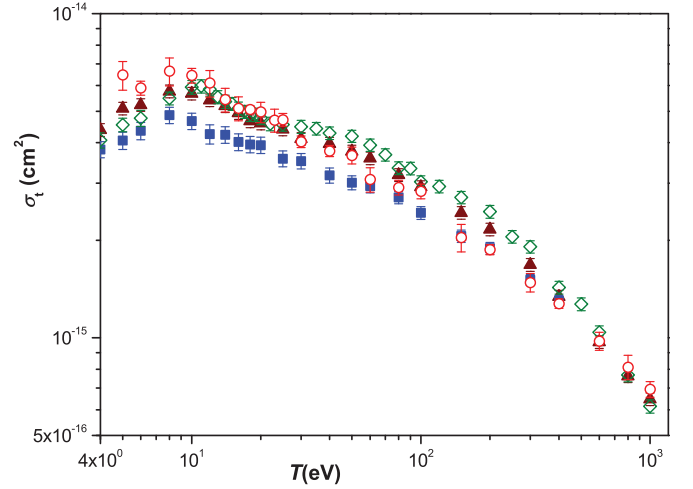


FIG. 3. (Color online) Present experimental results for pyrimidine (○) in comparison to TCS of benzene measured by (▲) Mozejko *et al.* [37], (■) Sueoka [38], and (◇) Makochehanwa *et al.* [42].

method described in Ref. [36]. Assuming that the dipole transition to the first rotational state ($0_0 \rightarrow 1_0$), whose excitation energy amounts to $E_{10} - E_{00} = 4.0 \times 10^{-2}$ meV, is the major transition, the electron-scattering cross section σ_{rot} due to rotational excitation was calculated using Eqs. (22) and (23) and added to σ_t calculated using Eq. (21).

IV. RESULTS AND DISCUSSION

The results of the present measurements are shown in Fig. 3 and listed in Table I. Apart from the weak shoulderlike

TABLE I. Total electron-scattering cross section σ_t of pyrimidine.

T (eV)	σ_t (10^{-16} cm 2)
5	64.61 ± 6.56
6	58.96 ± 2.91
8	66.42 ± 6.59
10	64.42 ± 3.36
12	61.03 ± 5.75
14	54.28 ± 4.52
16	51.02 ± 4.33
18	50.60 ± 1.39
20	49.69 ± 3.62
23	46.92 ± 3.81
25	47.04 ± 2.13
30	40.26 ± 1.65
40	37.71 ± 1.52
50	36.55 ± 2.20
60	30.80 ± 2.65
80	29.09 ± 1.52
100	28.32 ± 1.49
150	20.39 ± 1.99
200	18.73 ± 0.68
300	14.82 ± 0.98
400	12.76 ± 0.43
600	9.78 ± 0.63
800	8.13 ± 0.70
1000	6.94 ± 0.39

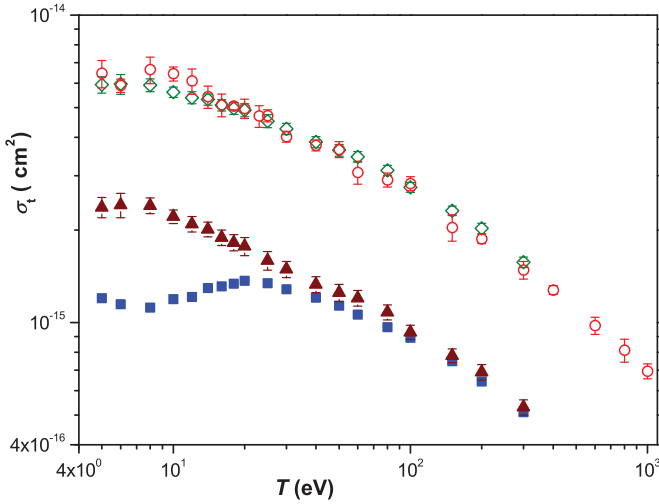


FIG. 4. (Color online) Experimental (O) TCS of pyrimidine in comparison to the semiempirical values (\diamond) obtained using the additivity rule [41]; (\blacktriangle) TCS of C_2H_2 [39]; (\blacksquare) TCS of N_2 [40].

structure at energies around 10 eV, the TCS of pyrimidine decreases with increasing electron energy. Since there are no experimental data for the TCS of pyrimidine measured by other groups, the present results are compared to the TCS of benzene. The TCS of both molecules are expected to agree approximately at the intermediate and high electron energies because they are isoelectronic and have a similar structure. It is evident from Fig. 3 that the present results are well reproduced by the benzene data of Mozejko *et al.* [37], even at low electron energies, while those of Sueoka [38] are noticeably lower than the TCS of pyrimidine at electron energies below 50 eV. It should be noted that the disagreement between both data at low electron energies is more realistic as the relatively high dipole moment of pyrimidine, which is one order of magnitude greater than that of benzene, leads to a strong elevation of the TCS in the low-energy region.

In addition to the TCS of benzene, the present results are in Fig. 4 compared to the semiempirical values which were obtained using the TCS of C_2H_2 [39], N_2 [40], and the additivity rule [41]. As can be seen from Fig. 4, the experimental and semiempirical values agree within the experimental uncertainties over the whole energy range, even at electron energies lower than 20 eV. The good agreement in the low-energy range is not expected since the electron scattering caused by the rotational excitation due to the high dipole moment is not taken into account in the semiempirical values. Furthermore, the additivity rule [41] is generally only valid at intermediate and high electron energies.

Figure 5 shows the elastic and inelastic electron-scattering cross sections calculated using the theoretical method described above for electron energies between the first ionization potential of pyrimidine located at about 10 eV [6] and 1 keV. However, it should be noted that the present theoretical cross sections below 20 eV are questionable because of the limited validity of the SCOP model in the low-energy region [22]. The inelastic-scattering cross sections are compared to the total ionization cross sections that were computed using the BEB model [10]. The model uses the binding energy B_i , the average electron kinetic energy U_i , and the electron occupation

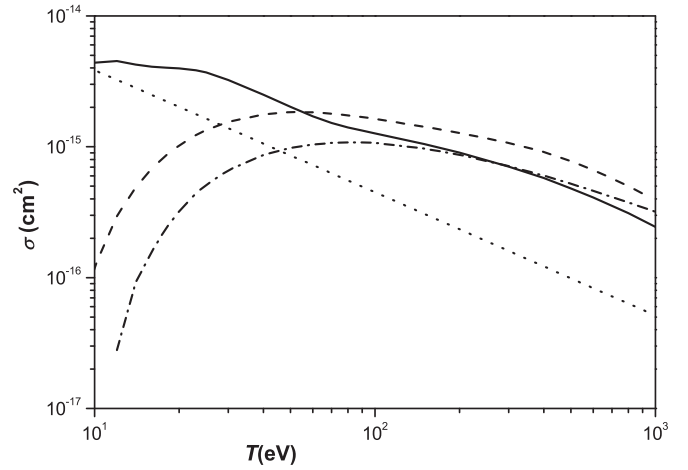


FIG. 5. Electron-scattering cross sections σ of pyrimidine calculated using the SCOP model [9]: (—) elastic-scattering cross section, (---) inelastic-scattering cross section, (-·-·-) ionization cross section, and (····) electron-scattering cross section arising due to rotational excitations.

number N_i to calculate the partial ionization cross sections σ_i of the i th molecular orbital:

$$\sigma_i(t_i) = \frac{4\pi a_0^2 N_i (R/B_i)^2}{t_i + u_i + 1} \times \left[\frac{\ln t_i}{2} \left(1 - \frac{1}{t_i^2} \right) + 1 - \frac{1}{t_i} - \frac{\ln t_i}{t_i + 1} \right], \quad (24)$$

where $t_i = T/B_i$, $u_i = U_i/B_i$, a_0 is the Bohr radius, and R is the Rydberg energy. The total ionization cross section σ_{ion} is then obtained by summing up the partial ionization cross sections of the molecular orbitals:

$$\sigma_{\text{ion}}(T) = \sum_{i=1}^{N_o} \sigma_i(t_i), \quad (25)$$

where N_o is the number of the occupied molecular orbitals. The values of the binding energy B_i and of the average electron kinetic energy U_i were determined by means of the quantum chemical code GAUSSIAN 09 [24] deploying the 6-311G** set.

Apart from the shoulderlike structure of the elastic-scattering cross section at electron energies around 20 eV, the three cross sections depicted in Fig. 5 show usual energy dependence. The inelastic scattering and ionization cross sections rise up to a maximal value located around 80 eV and then decrease monotonically with increasing energy. As can be seen from Fig. 5, the difference between the inelastic scattering and total ionization cross section, corresponding to the excitation cross section, decreases with increasing electron energy, in accordance with the fact that inelastic scattering at high electron energies occurs predominantly due to ionization processes.

Figure 6(a) shows the present experimental results in comparison to the theoretical TCS of pyrimidine obtained by summing the elastic- and inelastic-scattering cross sections depicted in Fig. 5. The solid and dashed lines represent the theoretical values with and without the contribution of rotational excitations to the electron scattering, respectively.

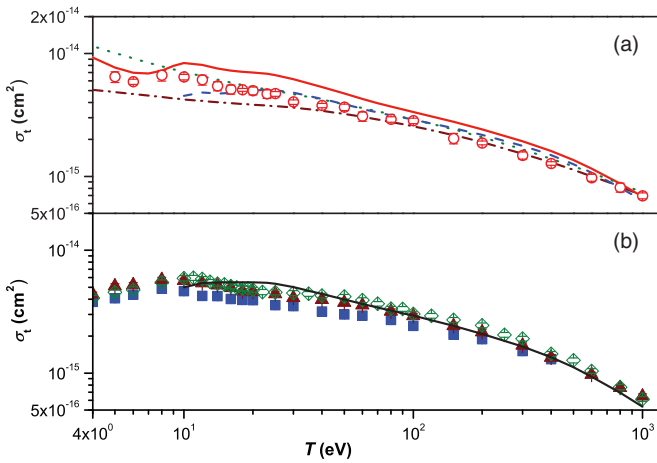


FIG. 6. (Color online) (a) Present experimental TCS (\circ) of pyrimidine in comparison to the theoretical values ($—$) obtained using the SCOP model [9]: ($- - -$) theoretical values without the contribution of rotational excitations to the electron scattering, ($- \cdot - \cdot -$) semiempirical data of Zecca *et al.* [6] without rotational excitations, and (\cdots) semiempirical data of Zecca *et al.* [6] including rotational excitations. (b) Theoretical TCS ($—$) of benzene calculated by means of the SCOP model [9] in comparison to experimental data: (\blacktriangle) Mozejko *et al.* [37], (\blacksquare) Sueoka [38], and (\diamond) Makochekanwa *et al.* [42].

Despite the limited validity of the SCOP model below 20 eV [22], the theoretical values including the contribution of rotational excitations are shown for electron energies down to 4 eV for the sake of completeness in comparing with the available experimental data. Since the predominant part of electron scattering by pyrimidine below 20 eV arises due to rotational excitations, it is to be expected that the qualitative feature of the energy dependence in the low-energy range is not interfered by the inaccuracy of the SCOP model. Additionally, the present experimental values are compared to the data of Zecca *et al.* [6] who employed the independent-atom screened additivity rule [7,8] and also the Born approximation in determining the rotational excitation cross sections.

If the contribution of rotational excitations is included, the experimental data are generally lower than the present theoretical TCS, while they are qualitatively well reproduced by the results of Zecca *et al.* [6] for electron energies down to 10 eV. The greatest deviation between the present experimental and theoretical data was found at electron energies around 30 eV where the theoretical values are about 50% higher than the experimental results. Above 30 eV, the deviation between both data decreases with increasing energy to vanish at high electron energies. It is also evident from Fig. 6(a) that the present theoretical TCS without the contribution of the rotational excitation reproduce the experimental data qualitatively well in the energy range between 20 eV and 1 keV, suggesting that the contribution of rotational excitations to the TCS of pyrimidine may either be overestimated in the present calculation or not resolved in the measurement, which would lead to a lowering of the experimental TCS. The latter can be caused by the finite angular and energy resolution of the electron energy analyzer that are not sufficient to discriminate against the electrons scattered due to rotational excitations.

In order to investigate the influence of rotational excitations on the deviation between the experimental and theoretical values, TCS of benzene, which has no permanent dipole moment because of its symmetry and therefore vanishing rotational excitation cross sections for electrons, were calculated using the SCOP model and compared to the experimental data measured by the Gdańsk group [37]. The experimental data of the Gdańsk group were chosen for the comparison because their experimental setup, consisting of a linear transmission apparatus and an electron-energy analyzing device with an angular resolution of 0.7 msr is similar to that used in this work.

It is evident from Fig. 6(b) that the experimental TCS of benzene by Mozejko *et al.* [37] are reproduced by the present theoretical data almost within the experimental uncertainties over the entire energy range, apart from the energy region around 25 eV, where both data deviate up to 15% from each other. A good agreement could also be found between the present theoretical values and the experimental results of Makochekanwa *et al.* [42]. However, the data of Sueoka [38] deviate significantly from the present theoretical values for electron energies up to 200 eV.

The good agreement of the theoretical TCS of benzene with the measured results of the Gdańsk group [37] whose experimental setup was similar to that of this work supports the assumption that the discrepancy between the present theoretical and experimental data for pyrimidine may mainly arise due to insufficient resolving power of the present apparatus with respect to the electron-scattering processes caused by rotational excitations. Indeed, the angular distribution of these processes is sharply peaked in the forward direction. According to the estimate carried out using the formula for the differential cross section given in Ref. [35], the part of electrons scattered due to rotational excitations within the detection solid angle of the present experiment makes up about 60%–70% of the total rotational excitation cross section at electron energies around 30 eV. Apart from rotational excitations, nonresolved vibrational transitions and the counting of electrons scattered at metallic surfaces such as slits and apertures which can result in an effective detection solid angle being larger than the geometrically defined one can lead to a decrease of the measured TCS.

V. CONCLUSION

Total electron-scattering cross sections of pyrimidine were measured for electron energies from 5 eV to 1 keV by means of a linear transmission device. The results of this work agree surprisingly well with the semiempirical values obtained using the additivity rule [41] and with the experimental TCS of the isoelectronic molecule benzene determined by Mozejko *et al.* [37] over the whole measured energy range. The good agreement, particularly at low electron energies, is remarkable since one expects the relatively high permanent dipole moment of pyrimidine to strongly increase its TCS with decreasing electron energy when compared to the case of the TCS of benzene and of the semiempirical values.

The present experimental data are rather well reproduced by the theoretical values of Zecca *et al.* [6] that were obtained

using the independent-atom screened additivity rule [7,8] including the contribution of rotational excitations to the electron scattering. On the other hand, the theoretical TCS of pyrimidine calculated with the SCOP model [9] that employs the molecular electron density distribution and is therefore expected to be more accurate than the IAM-SCAR model [7,8] deviate significantly from the experimental data at low electron energies if rotational excitations are taken into account.

The similar energy dependence observed between the present TCS of pyrimidine and the TCS of benzene [37], particularly at low electron energies, the qualitatively good agreement between the experimental data and theoretical results for pyrimidine when disregarding rotational excitations, and the good reproduction of the experimental TCS by the

theoretical results in the case of benzene suggest that the electrons scattered due to rotational excitations may be incompletely filtered out in the present measurement. For the precise measurement of the TCS of molecules with high permanent dipole moments, an experimental setup with a high angular and energy resolving power or an accurate determination of $\Delta\sigma_{el}$ including rotational excitations is therefore envisaged.

ACKNOWLEDGMENT

This work was carried out within the EMRP joint research project BioQuaRT. The EMRP is jointly funded by the EMRP participating countries within EURAMET and the European Union.

-
- [1] D. T. Goodhead, *Int. J. Radiat. Biol.* **65**, 7 (1994).
 [2] W. Y. Baek, M. Bug, H. Rabus, E. Gargioni, and B. Grosswendt, *Phys. Rev. A* **86**, 032702 (2012).
 [3] A. Zecca, C. Perazzolli, and M. J. Brunger, *J. Phys. B* **38**, 2079 (2005).
 [4] P. Mozejko, E. Ptasńska-Denga, A. Domaracka, and C. Szmytkowski, *Phys. Rev. A* **74**, 012708 (2006).
 [5] M. Fuss, A. Muñoz, J. C. Oller, F. Blanco, D. Almeida, P. Limão-Vieira, T. P. D. Do, M. J. Brunger, and G. García, *Phys. Rev. A* **80**, 052709 (2009).
 [6] A. Zecca, L. Chiari, G. Garcia, F. Blanco, E. Trainotti, and M. J. Brunger, *J. Phys. B* **43**, 215204 (2010).
 [7] F. Blanco and G. Garcia, *Phys. Lett. A* **330**, 230 (2004).
 [8] F. Blanco and G. Garcia, *J. Phys. B* **42**, 145203 (2009).
 [9] A. Jain and K. L. Baluja, *Phys. Rev. A* **45**, 202 (1992).
 [10] Y.-K. Kim and M. E. Rudd, *Phys. Rev. A* **50**, 3954 (1994).
 [11] W. Y. Baek and B. Grosswendt, *J. Phys. B* **36**, 731 (2003).
 [12] A. E. Hughes and C. C. Phillips, *Surf. Interface Anal.* **4**, 220 (1982).
 [13] T. Edmonds and J. P. Hobson, *J. Vac. Sci. Technol.* **2**, 182 (1965).
 [14] T. Takaishi and Y. Sensui, *Trans. Faraday Soc.* **59**, 2503 (1963).
 [15] P. M. Craven and J. D. Lambert, *Proc. R. Soc. London, Ser. A* **205**, 439 (1951).
 [16] R. N. Nelson and S. O. Colgate, *Phys. Rev. A* **8**, 3045 (1973).
 [17] S. Hayashi and K. Kuchitsu, *J. Phys. Soc. Jpn.* **41**, 1724 (1976).
 [18] ISO, *Guide to the Expression of Uncertainty in Measurement* (International Organization for Standardization, Geneva, 1993).
 [19] J. B. Maljković, A. R. Milosavljević, F. Blanco, D. Šević, G. Garcia, and B. P. Marinković, *Phys. Rev. A* **79**, 052706 (2009).
 [20] P. Palihawadana, J. Sullivan, M. Brunger, C. Winstead, V. McKoy, G. Garcia, F. Blanco, and S. Buckman, *Phys. Rev. A* **84**, 062702 (2011).
 [21] R. E. Fox, W. M. Hickam, T. Kieldaas, Jr., and D. J. Grove, *Phys. Rev.* **84**, 859 (1951).
 [22] K. L. Baluja and A. Jain, *Phys. Rev. A* **45**, 7838 (1992).
 [23] N. Sanna and F. A. Gianturco, *Comput. Phys. Commun.* **128**, 139 (2000).
 [24] GAUSSIAN 09, Gaussian, Inc., Wallingford, CT.
 [25] S. Hara, *J. Phys. Soc. Jpn.* **22**, 710 (1967).
 [26] G. Staszewska, D. M. Schwenke, and D. G. Truhlar, *Phys. Rev. A* **29**, 3078 (1984).
 [27] G. Staszewska, P. Staszewski, and K. Żebrowski, *J. Electron Spectrosc. Relat. Phenom.* **162**, 56 (2008).
 [28] F. Calegro, *Variable Phase Approach to Potential Scattering* (Academic, New York, 1967).
 [29] A. Jain, *Phys. Rev. A* **34**, 3707 (1986).
 [30] A. Jain, *J. Chem. Phys.* **86**, 1289 (1987).
 [31] P. M. Patel, C. V. Pandya, and K. L. Baluja, *Fiz. A* **19**, 47 (2010).
 [32] C. V. Pandya and K. L. Baluja, *J. At. Mol. Sci.* **3**, 279 (2012).
 [33] J. D. Lambert, *Numerical Methods for Ordinary Differential Systems: The Initial Value Problem* (Wiley, New York, 1991).
 [34] A. Jain, *J. Phys. B* **21**, 905 (1988).
 [35] L. A. Collins and D. W. Norcross, *Phys. Rev. A* **18**, 467 (1978).
 [36] A. Jain and D. G. Thompson, *Comput. Phys. Commun.* **30**, 301 (1983).
 [37] P. Mozejko, G. Kasperski, C. Szmytkowski, G. P. Karwasz, R. S. Brusa, and A. Zecca, *Chem. Phys. Lett.* **257**, 309 (1996).
 [38] O. Sueoka, *J. Phys. B* **21**, L631 (1988).
 [39] O. Sueoka and S. Mori, *J. Phys. B* **22**, 963 (1989).
 [40] J. C. Nickel, I. Kanik, S. Trajmar, and K. Imre, *J. Phys. B* **25**, 2427 (1992).
 [41] J. W. Otvos and D. P. Stevenson, *J. Am. Chem. Soc.* **78**, 546 (1956).
 [42] C. Makochekanwa, O. Sueoka, and M. Kimura, *Phys. Rev. A* **68**, 032707 (2003).